Notched Strength Analysis of Tensile Specimens Taken From a Thick, Filament-Wound Graphite/Epoxy Pressure Vessel

by

Paul Gagnon

thesis submitted to the Faculty of the

Virginia Polytechnic Institute and State University

in partial fulfillment of the requirements for the degree of

Master of Science

in

Engineering Mechanics

APPROVED:

Dr. Don H. Morris, Chairperson

Dr. Norman Dowling

Dr. L. Glenn Kraige

March, 1987

Blacksburg, Virginia

Notched Strength Analysis of Tensile Specimens Taken From a Thick, Filament-Wound Graphite/Epoxy Pressure Vessel

by

Paul Gagnon

Dr. Don H. Morris, Chairperson

Engineering Mechanics

(ABSTRACT)

An experimental analysis of specimens taken from a thick, filament-wound composite material pressure vessel (cylinder) was performed by testing tensile coupons with various semi-elliptical surface notches. The strength of specimens with small notches was found to be notch insensitive. The strength of specimens with larger notches depended on the size of the notch.

The fracture toughness of the laminate was found by applying a general fracture-toughness parameter approach. Using this value, several approaches were employed to predict failure loads. The accuracy of the approaches depended on the size of the notches. In general, the linear-elastic fracture mechanics method overpredicted the failure strength of specimens with intermediate sized notches, but predicted failure strength accurately for specimens with large notches. A strength of materials approach accurately predicted notched strength only for specimens with small notches. Notched strength was more accurately predicted for all notch sizes using an empirical approach, with the notch area used to predict failure instead of the notch depth, which was used in the linear-elastic fracture mechanics and strength of materials approaches.

Acknowledgements

I would like to thank Dr. Don H. Morris for all the guidance he has given me and for all the patience he has shown me.

Thanks also go to Bob Simonds, whose help and friendship have been invaluable to me over the past few years, and to G. K. 'Mac' McCauley, for all of his help with the testing machines and the photography.

Finally, I would like to thank C. C. Poe, Jr. and NASA Langley Research Center for sponsoring this work.

Table of Contents

List of Figures

List of Tables

List of Symbols

a	flaw depth
A_n	notch area
A_o	cross-sectional area of unnotched specimen
B	specimen half-width
c	notch half-length at surface
E_x	laminate stiffness modulus in loading direction
E_y	laminate stiffness modulus in transverse direction
F_s	boundary correction factor
G_{xy}	laminate shear modulus
K_I	stress intensity factor
K_Q	critical stress intensity factor
P	applied tensile load
P_F	load at failure
Q	shape factor for an elliptical crack
Q_c	general fracture-toughness parameter
S	remote uniform tensile stress
t	thickness of specimen
ε_{iuf}	fiber failing strain
ν_{xy}	laminate Poisson's ratio
ξ_1	material constant
φ	parametric angle of the ellipse
σ_N	notched strength
σ_o	unnotched strength

Introduction

Laminated and filament-wound composite materials are being used on an increasing basis for advanced technological applications, including structural components on current military fighter planes, or as a possible solid rocket motor casing on the Space Shuttle. In such applications the reduction in strength of a damaged component is an area of concern. The National Aeronautics and Space Administration (NASA) Langley Research Center is sponsoring work at Virginia Polytechnic Institute and State University for the purpose of evaluating the notched strength of tensile specimens taken from a thick, filament-wound composite cylinder. The primary objective of this analysis was to develop a method of predicting the reduction in strength of a notched (damaged) member if the size of the damaged region is known. To achieve this, static tension tests were performed on specimens with various semi-elliptical notches in order to accumulate a data base and also to observe the damage accumulation process.

Literature Review

The notched strength analysis of a thick, filament-wound composite cylinder for possible space shuttle applications is currently a topic under research at NASA Langley Research Center. Recently, Poe, Illg, and Garber [1,2] conducted impact tests on the same filament-wound composite cylinder investigated in this report, using several different shaped objects and several different velocities for impacting their specimens. They modeled the damaged regions by using an equivalent semi-elliptical slit-like surface notch, the same type of notch investigated in this report.

Two methods of predicting failure loads for materials containing semi-elliptical surface notches are discussed in the literature. Newman and Raju [3] formulated empirical stress-intensity factor equations for semi-elliptical surface cracks using a three-dimensional finite element analysis. These equations are for isotropic, linear-elastic materials subjected to uniform tension in a finite width plate. Their approach uses a stress-intensity factor that is a function of notch depth, notch width, plate thickness, plate width, and ellipse angle.

Sendeckyj [4] derived equations which predicted the strength of a material with a semi-circular surface notch. Sendeckyj used an elementary mechanics of materials approach for isotropic, linear-elastic materials, and achieved good results when he used these equations to predict the failure of thin laminated composite specimens. Sendeckyj's strength value was a function of notch depth,

specimen thickness, radius of the semi-circular notch, and plate width. He assumed uniform tensile loading and a linear stress distribution through the thickness of the specimen at the notch.

Both the Newman-Raju and Sendeckyj solutions were used to predict the notched strength of the filament-wound composite cylinder with semi-elliptical surface notches. Harris and Morris [5,6] found that thicker composite materials (thickness greater than 0.4 in.) behaved as would a thick, isotropic, linear-elastic material in some loading situations, which resulted in the use of the Newman-Raju and Sendeckyj solutions.

Materials and Methods

Test specimens were obtained from a scaled 30 in. diameter, full-thickness cylinder. The cylinder was wound with filaments 90 degrees to the filaments in the full-size cylinder. This was done so that the specimens would not be curved, and so that the uniform applied tension on the specimens would be in the higher stress hoop direction of the full-size cylinder, which is the longitudinal direction of the scaled cylinder. The layers of the scaled cylinder, from the cylinder exterior (front face of the specimen) to the cylinder interior (back face), are

$$(\pm 56.45°)_2/0°_3/[(\pm 56.45°)_2/0°_3]_3/[(\pm 56.45°)_2/0°_3]_7/(\pm 56.45°/0°_6)_4/(\pm 56.45°)_2/(90°/0°)\ ,$$

with the underlined $\pm$ 56.45° layers 1.6 times as thick as the other layers. In the full-size cylinder, the fibers are Hercules, Inc. AS4W-12K, and the winding resin is Hercules, Inc. HBRF-55A. In the scaled cylinder, the 0 degree layers were hand laid with unidirectional broadgoods which consisted of the same fiber used in the full-size cylinder and a compatible resin (Hercules MX-16).

The specimens, provided by NASA Langley, are 12 in. x 2 in. x 1.4 in. filament-wound graphite/epoxy coupons with the nonsymmetric stacking (winding) sequence shown previously. The dimensions varied insignificantly from specimen to specimen, so the above nominal dimensions are used for all calculations. Since the specimens were cut from a cylinder, they have slightly curved

parallel front and back faces. In order to insure proper gripping, aluminum spacers, which were 4 in. x 2 in., were used to compensate for this curvature (Figure 1). 3M Type 21 Wetordry Fabricut fine mesh grit sandpaper was inserted between the spacers and the specimens to aid gripping. Tension tests were conducted on a Baldwin-Tate-Emery hydraulic testing machine which had a 120 kip load limit. Fiske Refining Company Lubriplate 130-AA grease was applied between the wedge-action grips and the machine crosshead. Using this instead of graphite dust or oil allowed for higher load levels to be reached and also resulted in reduced grip slippage. More information on gripping and testing thick composite materials can be found in reference 7.

NASA Langley Research Center provided the specimens, which already had the semi-elliptical notches machined into the surface. The semi-elliptical notches were machined into the front face of the specimen using an ultrasonic cutting tool with 0.0016 in. width. The plane of the notch is oriented perpendicular to the loading direction.

Specimens had either 2 in. gage sections (2B = 2) (Figure 1) or 1 in. gage sections (2B = 1) (Figure 2). The 2B = 1 gage sections were created by grinding out the sides of the specimen with a 9.25 in. radius grinding wheel. The failure load of specimens with small notches would have exceeded the load capacity of the machine if the 2 in. gage section was used. There were six different notch sizes tested; five required the smaller 1 in. gage section. There were 3 replicates for each of the six notch sizes. The first set of replicates were subjected to static tension tests at a constant crosshead displacement rate of 0.01 in. per minute in order to obtain failure loads. The second replicate of each specimen type was pulled in tension to 85, 90, and 95 percent of the failure load found in the first replicate test. At each load level, the specimen was removed from the testing machine to be x-rayed for damage. Zinc Iodide was used to enhance the x-rays. An ample period of time (minimum of 1/2 hour) was allowed for the Zinc Iodide to propagate into the damaged region. The specimen surface was then cleaned with acetone so that no Zinc Iodide, which could possibly damage the x-ray film, was left on the specimen surfaces. Two x-rays, one through-the-thickness (top view) and one through-the-width (side view) were taken for each specimen at each load level. The specimens were placed in a Hewlett-Packard 43805N X-Ray System (Faxitron Series) machine at a

distance of about 35 in. from the x-ray source, with Kodak Industrex M-5 X-Ray film placed directly under the specimen. X-rays through-the-thickness, with front surface up, were taken using 90 kVp of energy for 30 seconds. Side view x-rays were taken at the same energy for 20 seconds on the 1 in. (2B = 1) gage section width specimens and 40 seconds on the 2 in. (2B = 2) gage section specimens. The film was then developed according to Kodak instructions. Each specimen type was also x-rayed at failure.

The third replicate of each specimen type had strain gages placed on the front and back faces 1 in. above the notch and five additional gages placed along the edge in the plane of the notch (also Figure 1). The front and back gages were to check for bending; the edge gages were to monitor strain distribution through-the-thickness of the specimen. Strain gages were wired into a Vishay 2100 series strain gage amplifier, which was attached to a data acquistion analog to digital converter board produced by Data Translation, Inc., which was interfaced with an IBM PC. Strain values were recorded every 5 seconds and stored on a floppy disk. X-rays were taken, using the procedure indicated above, at 60 and 75 percent of the average failure load of the first two replicate tests. Failure loads were recorded.

The specimen test matrix is shown in Table 1. Specimens in this paper with identifying numbers beginning with a '4' were subjected to the above test procedure. Specimens with identifying numbers beginning with a '2' were specimens tested by Harris and Morris [6] in their preliminary testing. These specimens were tested in a similar manner as the first replicates in this report , and failure loads for these specimens were used along with data from this report.

The experimental data is presented in terms of notched strength and unnotched strength. The notched strength σ_N is defined in terms of the far field stress at failure, with $\sigma_N = P_F/2Bt$, where P_F is failure load, 2B is the width of the gage section, and t is the specimen thickness. The unnotched strength σ_o was determined by Poe [2] using the same equation as above, applied to tests on unnotched specimens. The value is $\sigma_o = 50.1$ ksi.

Results

The results for flaw aspect ratios (a/c values) of 2.0, 1.0, 0.5, and 0.175 are presented in Tables 2 through 5, respectively. Each table includes the flaw depth ratio (a/t), the specimen identification number, the gage section width (2B), the failure load of the specimen (P_F), the calculated notched strength of the specimen, and the ratio of notched strength to unnotched strength (σ_N/σ_o), which is used to normalize the data. The normalized notch area (A_N/A_o) is also presented in Tables 2 through 5, and is defined as the ratio of the notch area (area of the semi-ellipse) to the area at the gage section of an equivalent unnotched specimen, or

$$A_N / A_o = \pi ac/4Bt.$$

There were two different failure processes which occurred. Specimens with small notches ($a/t < 0.1$; $A_N/A_o < 0.02$) exhibited notch insensitive behavior. The specimens with small notches failed catastrophically into two distinct pieces, while specimens with larger notches experienced a type of failure known as notched layer failure.

Calculated notched strength of specimens which failed into two distinct pieces was about the same value as the unnotched strength, resulting in a strength ratio (σ_N/σ_o) of about 1.0, leading to the conclusion of notch insensitivity. Another indication of notch insensitivity is that some specimens

tested by Harris and Morris [6] failed catastrophically away from the notch. In the specimens with smaller notches, some small cracks occured around the notch (indicated by x-rays), but they did not propagate appreciably in any direction, and failure was sudden and parallel to the notch plane. The failure was complete, including breakage of all 56.45 degree and 0 degree plies. The splintered failure surface is shown in Figure 3.

The second failure mode, notched layer failure, occurred in specimens with larger notches (a/t > 0.1; A_N/A_o > 0.02) in both 1 in. and 2 in. gage section widths. These specimens failed in two stages. First, the part of the laminate which was cut by the notch failed at the notch and also de-laminated from the uncut layers (from the remaining ligament). Then, at a higher load level, the remaining ligament would fail (second stage).

The failure process progressed as follows for the notched layer failure (first stage). First, at about 50 to 60 percent of the failure load of a specimen, the front face strain, which had been increasing linearly with load, began to exhibit some nonlinear behavior. This would indicate that damage had occurred in the specimen, a presumption which was backed up by visual evidence of damage in the 60 percent x-rays taken in the third replicate tests. Damage then accumulated as shown in the 85 percent x-rays (Figure 4) and 90 percent x-rays (Figure 5). Cracking occurred in the 56.45 degree layers, and the damage increased as the load increased. The damage occurred in the notch region, as indicated by the face (top view) x-rays, and near the bottom of the notch, as indicated by the side view x-rays. As the load increased, the damage spread away from the notch in the direction of the specimen length and also propagated deeper into the thickness of the specimen. However, the damage would only penetrate into the thickness until it intersected with a 0 degree layer. Then it propagated along the 0 degree layer in both directions down the length of the specimen, as shown in the 90 percent x-ray (Figure 5) and the 95 percent x-ray (Figure 6).

The notched layer then failed in the following manner. A large snapping sound would occur as the notched layer separated from the rest of the specimen along the damage inhibiting 0 degree layer. The notched layer separated down the length of the specimen into the gripping region. These

characteristics of notched layer failure are shown in the x-rays in Figure 7. The front face strain dropped significantly, signifying the unloading of the notched layer as it fractured. The load at this point of the test was taken to be the failure load of the specimen. The remaining ligament of the specimen, that below the 0 degree layer, remained essentially intact and primarily undamaged. A model to predict the remaining ligament failure (second stage) was developed by Poe [2].

The x-rays of the specimens at any load typically show the accumulation of the damage through either the thickness or the width. In order to further examine the failure surface, the notched layer of the specimens in the second replicate group was removed from the remaining ligament, revealing detail from the fracture surface not evident in the x-rays. This was done by slicing the specimens, with a bandsaw specifically bladed for composite material cutting, approximately 1.0 in. above and below the notch in a plane parallel to the notch. The notched layer was then pulled off, revealing the damage surface (Figure 8). The cracked 56.45 degree layers are clearly visible. The bottom of the notch, which is a probable site of damage initiation (as indicated by previous x-rays), is visible in the top 56.45 degree layer. The cracking is evident through successive 56.45 degree layers deeper into the thickness of the specimen, and the damage occurred further away from the notch as it progressed deeper into the specimen. Damage did not penetrate the 0 degree layer below the notch.

As previously mentioned, the specimens in the third replicate group were instrumented with seven strain gages, two on the faces and five along the edge. The front face gage indicated damage during loading and also indicated unloading of the notched layer at failure. The back face gage, in conjunction with the front face gage, indicated a small amount of bending associated with the each test, probably due to the anisotropy of the laminate. This bending, according to Poe [2], is small enough to discount. The five edge gages were used in order to determine the strain distribution through the thickness of the specimen. No consistent pattern developed for the six specimens tested; additional replicates are necessary in order to obtain any significant results from these gages.

Discussion

Two analytical solutions, formulated by Newman and Raju [3] and Sendeckyj [4] , were utilized in order to quantify the experimental results. Both are based on isotropic, linear-elastic materials, which the material in this report is not. However, Harris and Morris [5] have found that thicker composite laminates tend to exhibit isotropic, linear-elastic behavior, a presumption which leads to the utilization of these two solutions.

Newman and Raju [3] have generated solutions for semi-elliptical surface notches present in a finite width plate. They generated equations which provide a stress-intensity factor for a given material and geometry. These empirical equations were generated by a three-dimensional finite element analysis, and are of the form

$$K_I = S(\pi a/Q)^{1/2} F_s\,(a/c,\ a/t,\ c/B,\ \varphi) \qquad (1)$$

where K_I , the stress-intensity factor, depends on notch depth (a), notch width (2c), specimen thickness (t), specimen width (2B), ellipse parametric angle (φ), remote uniform tensile stress (S), and ellipse shape factor ($Q = Q(a/c)$).

It is desired to predict the failure strength of the laminate, σ_N. Rearranging equation (1) and noting that σ_N = S and that K_Q is defined as the fracture toughness, or critical stress-intensity (at failure) yields

$$\sigma_N = K_Q/F_s(\pi a/Q)^{1/2} \qquad (2)$$

The preliminary unknown in equation (2) is K_Q, the fracture toughness. A value for K_Q was estimated using Poe's general fracture-toughness parameter [8] , which was developed for laminated composites. The relationship between the general fracture-toughness parameter (Q_c) to the fiber failing strain (ε_{tuf}) was found by Poe [8] to be relatively constant for all laminates, and is defined as

$$Q_c/\varepsilon_{tuf} = 0.298\ in.^{1/2} \qquad (3)$$

where

$$Q_c = K_Q\xi_1/E_x \qquad (4)$$

and

$$\xi_1 = 1\text{-}\nu_{xy}\,(E_y/E_x)^{1/2}\,. \qquad (5)$$

In equation (5),

E_x = the laminate stiffness modulus in the loading direction

E_y = the laminate stiffness modulus in the transverse direction

and

ν_{xy} = the laminate inplane Poisson's ratio.

The laminate material properties were calculated using laminate analysis theory [2] and are

E_x = 4.442 x 10^6 psi

E_y = 5.656 x 10^6 psi

G_{xy} = 2.862 x 10^6 psi

and

ν_{xy} = 0.3509.

Using equation (5), the value of ξ_1 was determined to be

ξ_1 = 0.6040.

The fiber failing strain, ε_{tuf}, was estimated by Harris and Morris [6] from the unnotched strength by

$\varepsilon_{tuf} = \sigma_o/E_x$ = 50.1 x 10^3 / 4.442 x 10^6 = 0.0113.

Applying this value to equations (3) and (4) yields a critical stress-intensity K_Q of 24.7 ksi $in.^{1/2}$. This value, combined with equation (2), allows for a predicted value of notched strength for a given notch size.

Predictions for all notch aspect ratios (a/c values) are shown in Figures 9 through 11. Each plot is for a constant value of a/c, with the notch depth ratio (a/t) as the variable; the notched strength was normalized by the unnotched strength (σ_N/σ_o). It should be noted that the Newman-Raju equation (1) is valid only for certain ranges of a/c and c/B. The parametric angle φ yields a minimum predicted strength at a value of either 0 degrees of 90 degrees. The value of φ was determined to be 0 degrees if c/a < 1.2 and 90 degrees if c/a > 1.2 . Strength ratio values greater than 1.0 which

resulted from the Newman-Raju solutions were reduced to 1.0 since the notched strength should not exceed the unnotched strength. Discussion of correlation between predictions and experimental data will follow presentation of the second analytical solution.

Sendeckyj [4] formulated analytical solutions for semi-circular surface notches in laminated composites using a strength of materials approach. The equations had to be rederived using a semi-elliptical notch geometry in place of the semi-circular geometry. A linear stress distribution at the plane of the notch was assumed. The resulting equation, as in the case of the semi-circular notch, depends solely on the notch geometry, and the resulting strength ratio depends only on notch geometry and unnotched strength. Sendeckyj [4], using equilibrium equations, found the strength ratio to be given by

$$\sigma_N / \sigma_o = (BF-CE)/(AF-CD + t(BD-AE))$$

where

$$A = 2Bt$$

$$B = 2Bt - \pi ac/2$$

$$C = Bt^2 - 2ca^2/3 - \pi act/2$$

$$D = Bt^2$$

$$E = C$$

and

$$F = 2Bt^3/3 - 4ca^2t/3 - \pi act^2/2 - \pi ca^3/8$$

with 2B, a, c, and t being the same quantities as previously defined. Strength ratio is plotted against notch depth ratio in Figures 9 through 11 for the Sendeckyj solution and the Newman-Raju solution, again with the notch aspect ratio fixed for each plot. Predictions for both solutions are shown for both width values of 2B = 1 and 2B = 2. There was not enough experimental data to draw any conclusive results from the a/c = 0.175 specimens; therefore, the Newman-Raju and Sendeckyj solutions are not shown for this value.

There are three distinct ranges with different degrees of correlation for the Newman-Raju solutions. For shallow notches (a/t < 0.1) the notch insensitivity of the material is evident, as shown by the strength ratio of the specimen typically being a value of about 1.0. The prediction for strength of specimens with deep notches (a/t > 0.2) is quite good, as shown by the a/c = 2.0 graph (Figure 9) and the a/c = 1.0 graph (Figure 10). There is, however, poor correlation in the range between a/t = 0.1 and a/t = 0.2. This is shown by the strength overprediction in the a/c = 1.0 graph (Figure 10) and the a/c = 0.5 graph (Figure 11).

The Sendeckyj solution has two distinct ranges with different degrees of correlation. For small notches (a/t < 0.1) there is good correlation between the solution and the experimental data for all three a/c values. There is some correlation for the a/c = 2.0 data (Figure 9) and the Sendeckyj solution for deeper notches (a/t > 0.1), but the agreement is not consistent for all a/c values. There is little correlation for a/c = 1.0 (Figure 10) and a/c = 0.5 (Figure 11) for any notch depth a/t > 0.1. For these two cases, there is a large overprediction of strength. In general, the Sendeckyj solution is not accurate in predicting the failure of the material tested. The Newman-Raju method predicts strength well for large notch depths, but there is a region where an overprediction of strength occurs. Poe [1] noted that the discrepancy between data and prediction in the intermediate ranges of flaw depth ratio (0.1 < a/t < 0.2) was probably caused by the anisotropy of the notched layers affecting the stresses around the crack, violating the isotropic assumptions of the two methods. For deeper notches, Poe felt that the thicker notched layer behaved more isotropically, resulting in better correlation between data and experiment for the Newman-Raju approach. The degree of correlation for each method is shown for all the data in Figures 12 (Newman-Raju) and

13 (Sendeckyj), which show predicted notched strength ratio plotted against the measured value. Comparing these figures, it is evident that the Newman-Raju prediction is more accurate than the Sendeckyj prediction over the entire range of data.

The previous solutions were primarily dependent on notch depth and notch width. It became evident during evaluation of the testing results that the strength of a particular specimen could be more dependent on the notch area (A_N) than the notch width or depth. This motivation, coupled with the desire to be able to predict the strength of any specimen using a single relationship between strength and geometry, led to an empirical analysis of this particular material. The best correlation was obtained using a logarithmic relationship between notch area ($A_N = \pi ac/2$) and strength. The notch area was normalized with the cross-sectional area of an unnotched specimen, A_o ($A_o = 2Bt$). The equation relating σ_N / σ_o to A_N / A_o was found by performing a linear regression on all of the data associated with specimens which experienced notched layer failure and excluding data associated with specimens which experienced two-piece catastrophic failure. The resulting relationship is

$$\sigma_N / \sigma_o = -0.438 \times \log(A_N/A_o) + 0.161 \qquad (6)$$

The correlation coefficient associated with the linear regression is -0.93 (-1.0 is perfect). Again, all predicted strength ratios larger than 1.0 were reduced to 1.0, since the notched strength cannot exceed the unnotched strength. The equation predicts the behavior of this particular material accurately for all notch areas in specimens which experience notched layer failure in the range of areas tested ($0.0189 < A_N/A_o < 0.265$), for all notch aspect ratios tested (a/c = 2.0, 1.0, 0.5, and 0.175); for all notch depth ratios in specimens which experienced notched layer failure ($0.0920 < a/t < 0.491$), and for both widths considered (2B = 1 and 2B = 2). Whereas the Newman-Raju and Sendeckyj solutions have regions of poor correlation, this area based method predicts failure load well for all notch geometries tested. Also, the data base confirming the accuracy of the area based method is large, because all a/c values are modeled by one equation, as illustrated in Figure 12.

Conclusions

The Newman-Raju solution provided a better strength prediction than the Sendeckyj solution, most likely because the Newman-Raju utilizes material properities in the analysis, whereas the Sendeckyj solution does not. Both methods were developed for isotropic, linear-elastic materials which fail parallel to and in the plane of the notch. The notched layer failure which occurs in this type of specimen is different from the failure mode associated with both solutions, and this could effect the accuracy of the solutions. The Newman-Raju solution predicted strength well for notches with large depths ($a/t > 0.2$). There was poor correlation for mid-range notch depths ($0.1 < a/t < 0.2$); the solution overpredicted the strength. The Sendeckyj solution predicted strength most accurately for small notches, but the degree of correlation for notch depths of $a/t > 0.1$ is poor. The best correlation for all ranges of notch depth, notch width, specimen thickness, and specimen width was found using an empirical fit to the experimental data. It should be noted that no attempt was made to extend the results of this work involving experiments on tensile specimens to the failure of a thick, filament-wound pressure vessel.

The Newman-Raju and Sendeckyj solutions were adapted to use notch area instead of notch width and depth, but the results of either solution were not simplified to any degree, nor were there any gains in accuracy.

More research needs to be done in order to determine the underlying causes of the failure process, especially how they relate to the failure of a thick, filament-wound pressure vessel. Also, it should be noted that only notched layer failure was considered in this research. No attempt was made to model the remaining ligament failure.

Summary

The behavior of specimens with different semi-elliptical notch geometries subjected to uniform tensile loading was evaluated for a thick, filament-wound, graphite/epoxy composite material. The strength ratios were found by averaging the notched strengths of the three replicate tests. These three values typically varied by less than 10 percent. Two failure modes were exhibited during testing. Specimens with smaller notches (a/t $<$ 0.1; A_N / A_o $<$ 0.02) exhibited notch insensitive behavior, and typically failed catastrophically into two separate pieces. Other specimens with deeper notches exhibited a notched layer failure, with the notched layer of the specimen breaking and separating from the remaining ligament of the specimen. Failure of this remaining ligament was not considered in this report.

Poe's general fracture toughness parameter was utilized in order to find a fracture toughness, or critical stress-intensity factor. This value was used in order to predict notched strength using a finite element based solution derived by Newman and Raju. An analytical solution from Sendeckyj was adapted to the semi-elliptical notch geometry and was also employed to predict notched strength. Neither solution accurately predicted the notched strength for all notch depths.

The failure of the specimens exhibited a dependence on notch area, and an empirical approach was attempted incorporating this trait. A relationship between notch area and notched strength was

established which accurately predicted the notched strength of this material under the given testing conditions. Again, it should be noted that no attempt was made to extend the results of this work involving experiments on tensile specimens to the failure of a thick, filament-wound pressure vessel.

BIBLIOGRAPHY

1. Poe, C. C., Jr., Illg, W., and Garber, D. P., 'A Program to Determine the Effect of Low Velocity Impacts on the Strength of the Filament Wound Rocket Motor Case for the Space Shuttle,' NASA Technical Memorandum 87588, National Aeronautics and Space Administration, 1985.

2. Poe, C. C., Jr., Illg, W., and Garber, D. P., 'Tension Strength of a Thick Graphite/Epoxy Laminate After Impact by a 1/2-In.-Radius Impactor,' NASA Technical Memorandum 87771, National Aeronautics and Space Administration, 1986.

3. Newman, J. C., Jr., and Raju, I. S., 'Stress-Intensity Factor Equations for Cracks in Three-Dimensional Finite Bodies,' Fracture Mechanics: Fourteenth Symposium-Volume 1: Theory and Analysis, ASTM STP 791, J. C. Lewis and G. Sines, Eds., American Society for Testing and Materials, 1983, pp. I-238-I-265.

4. Sendeckyj, G. P., 'Some Observations on Fracture Behavior of Advanced Fiber-Reinforced Laminates,' Proceedings of the 12th Annual Meeting of the Society for Engineering Science, University of Texas at Austin, Oct. 20-22, 1975, pp. 625-634.

5. Harris, C. E., and Morris, D. H., 'Fracture of Thick Graphite/Epoxy Laminates with Part-Through Surface Flaws,' Composite Materials: Fatigue and Fracture, ASTM STP 907, H. T. Hahn, Ed., American Society for Testing and Materials, 1980, pp. 100-114.

6. Harris, C. E., and Morris, D. H., 'Preliminary Report on Tests of Tensile Specimens with a Part-Through Surface Notch for a Filament Wound Graphite/Epoxy Cylinder,' NASA Contractor Report 172545, National Aeronautics and Space Administration, 1985.

7. Harris, C. E., and Morris, D. H., 'Unique Aspects of Conducting Strength Tests on Thick Composites,' Proceeding of the 1984 S. E. M. Fall Conference, Nov. 4-7, Milwaukee, Published by the Society for Experimental Mechanics, 1984, pp. 112-117.

8. Poe, C. C., Jr., 'A Unifying Strain Criterion for Fracture of Fibrous Composite Laminates,' Engineering Fracture Mechanics, Vol. 17, No. 2, 1983, pp. 153-171.

Table 1 Specimen Test Matrix

a/c = 2.0		a/c = 1.0		a/c = 0.5		a/c = 0.175	
a/t	2B(in.)	a/t	2B(in.)	a/t	2B(in.)	a/t	2B(in.)
0.0670	1.0	0.0355	1.0	0.0558	1.0	0.0355	1.0
0.0920	1.0	0.0446	1.0	0.0670	1.0	0.0446	1.0
0.123	1.0	0.0558	1.0	0.0920	1.0		
0.179	1.0	0.0920	1.0	0.123	1.0		
0.290	1.0	0.126	1.0	0.179	2.0		
0.402	1.0	0.176	1.0	0.231	2.0		
0.491	2.0	0.290	2.0				
		0.402	2.0				
		0.491	2.0				

Table 2 Experimental Data for a/c = 2.0

Sp. ID	a/t	A_N/A_o	2B(in.)	P_F(kips)	σ_N(ksi)	σ_N/σ_o
2-7	0.0670	0.00494	1.0	74.2	53.0	1.058
2-8				73.2	52.3	1.043
average				73.7	52.7	1.052
4-1	0.0920	0.00950	1.0	73.3	52.4	1.046
4-8				73.7	52.6	1.050
4-20				70.0	50.0	0.998
average				72.3	51.7	1.031
2-13	0.123	0.0166	1.0	67.6	48.3	0.964
2-14				67.4	48.1	0.960
average				67.5	48.2	0.962
2-28	0.179	0.0355	1.0	61.0	43.6	0.867
2-29				62.6	44.7	0.892
average				61.8	44.1	0.880
2-30	0.290	0.0921	1.0	43.2	30.9	0.617
2-31				47.0	33.6	0.670
average				45.1	32.3	0.645
2-36	0.402	0.178	1.0	37.8	27.0	0.539
2-37				34.8	24.9	0.497
average				36.3	26.0	0.519
2-45	0.491	0.133	2.0	86.5	30.9	0.617
2-46				88.2	31.5	0.629
average				87.4	31.2	0.623

Table 3 Experimental Data for a/c = 1.0

Sp. ID	a/t	A_N/A_o	2B(in.)	P_F(kips)	σ_N(ksi)	σ_N/σ_o
2-21	0.0335	0.00247	1.0	77.5	55.4	1.106
2-22				73.2	52.3	1.043
average				75.4	53.9	1.076
2-23	0.0446	0.00439	1.0	76.1	54.4	1.086
2-26				80.6	57.6	1.150
average				78.4	56.0	1.118
2-27	0.0558	0.00684	1.0	73.7	52.6	1.050
2-34				75.4	53.9	1.076
average				74.6	53.3	1.064
4-13	0.0920	0.0189	1.0	62.0	44.3	0.884
4-18				55.9	39.9	0.796
4-23				58.5	41.8	0.834
average				58.8	42.0	0.838
4-3	0.126	0.0364	1.0	61.1	43.6	0.870
4-32				57.5	41.1	0.820
4-33				63.3	45.2	0.902
average				60.6	43.3	0.864
4-9	0.176	0.0701	1.0	47.9	34.2	0.683
4-21				50.4	36.0	0.719
4-42				45.0	32.1	0.641
average				47.8	34.1	0.681
2-12	0.290	0.0925	2.0	87.8	31.4	0.627
2-40				84.8	30.3	0.605
average				86.3	30.9	0.617
2-41	0.402	0.178	2.0	66.4	23.7	0.473
2-42				69.5	24.8	0.495
average				68.0	24.3	0.485
2-43	0.491	0.265	2.0	54.5	19.5	0.390
2-44				50.0	17.9	0.358
average				52.3	18.7	0.373

Table 4 Experimental Data for a/c = 0.5

Sp. ID	a/t	A_N/A_o	2B(in.)	P_F(kips)	σ_N(ksi)	σ_N/σ_o
2-17	0.0558	0.0136	1.0	66.9	47.8	0.955
2-18				70.3	50.2	1.002
average				68.6	49.0	0.978
2-19	0.0670	0.0198	1.0	70.0	50.0	0.998
2-20				67.1	47.9	0.956
average				68.6	49.0	0.978
4-14	0.0920	0.0379	1.0	55.7	39.8	0.794
4-15				54.0	38.6	0.770
4-22				50.5	36.1	0.721
average				53.4	38.1	0.761
2-2	0.123	0.0664	1.0	44.2	31.6	0.631
2-3				40.9	29.2	0.583
average				42.6	30.4	0.607
2-10	0.179	0.0707	2.0	86.5	30.9	0.617
2-11				92.5	33.0	0.658
average				89.5	32.0	0.639
4-26	0.231	0.122	2.0	68.4	24.4	0.488
4-27				63.8	22.8	0.455
4-28				73.3	26.2	0.523
average				68.5	24.5	0.488

Table 5 Experimental Data for a/c = 0.175

Sp. ID	a/t	A_N/A_o	2B(in.)	P_F(kips)	σ_N(ksi)	σ_N/σ_o
2-4	0.0355	0.0141	1.0	68.0	48.6	0.970
2-5				80.0	57.1	1.140
average				74.0	52.9	1.056
2-9	0.0446	0.0250	1.0	75.2	53.7	1.072
2-35				68.2	48.7	0.972
average				71.7	51.2	1.021

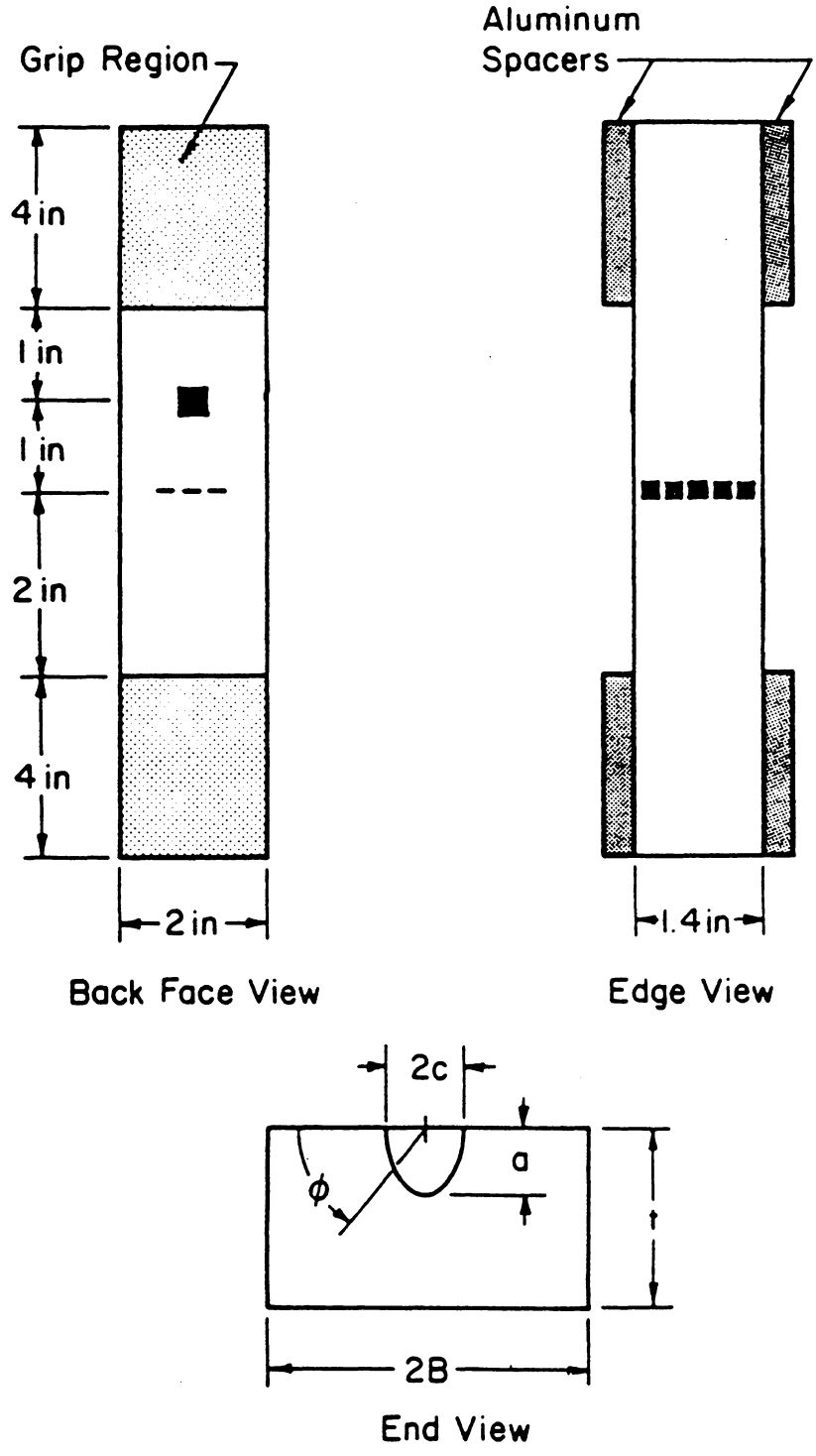

Figure 1. Illustration of Specimens with 2B = 2 in.

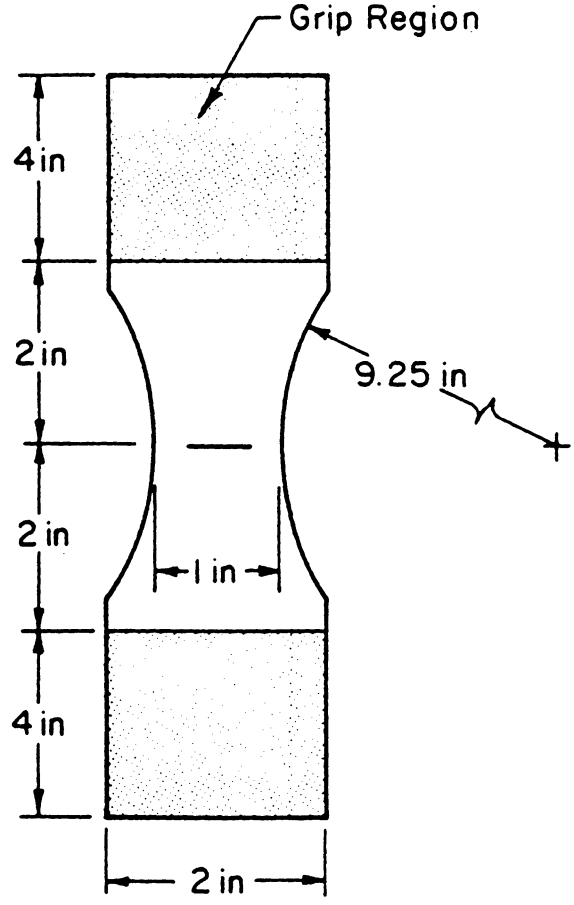

Figure 2. Illustration of Specimens with 2B = 1 in.

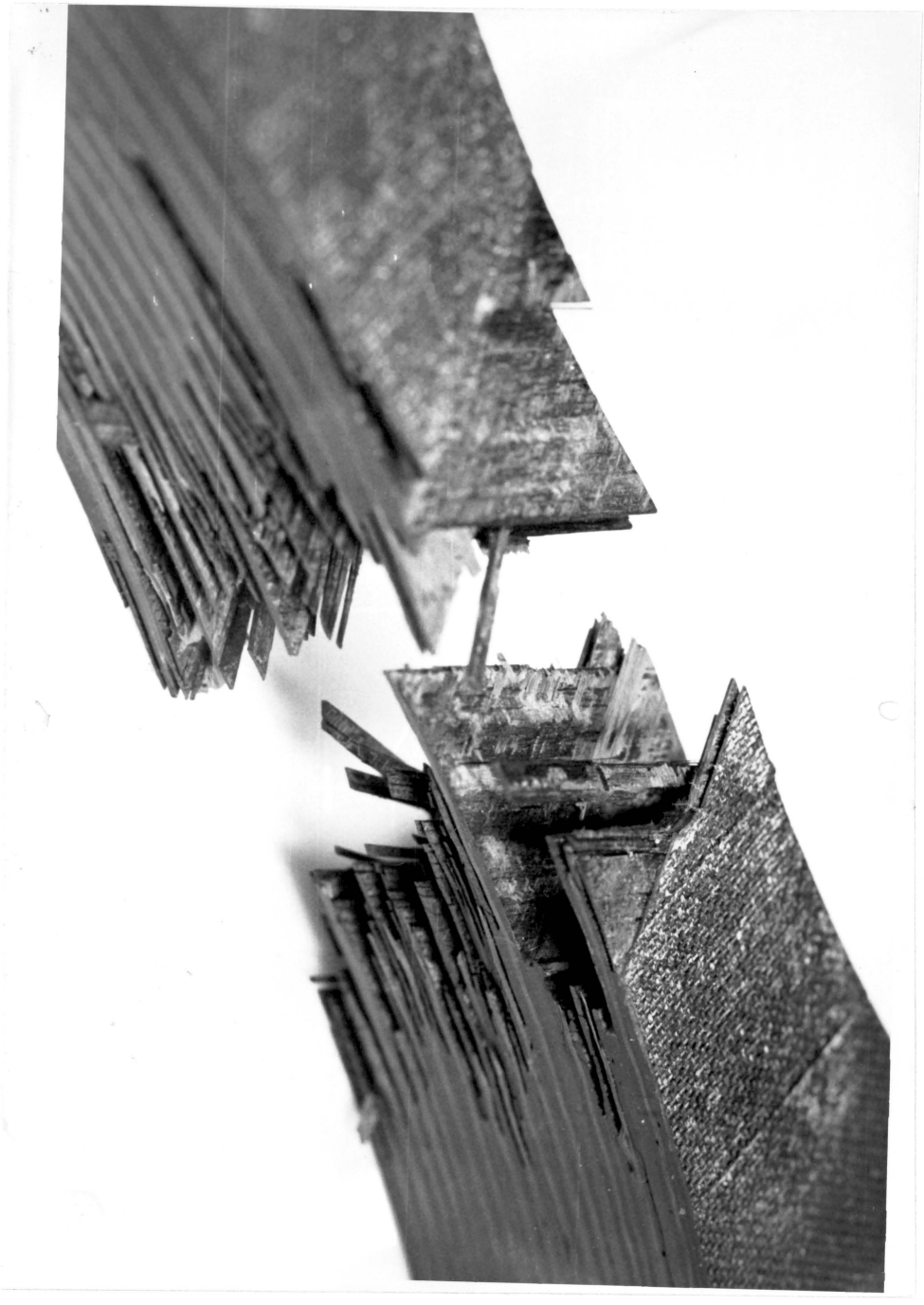

Figure 3. Photograph of Two-Piece Catastrophic Failure Surface

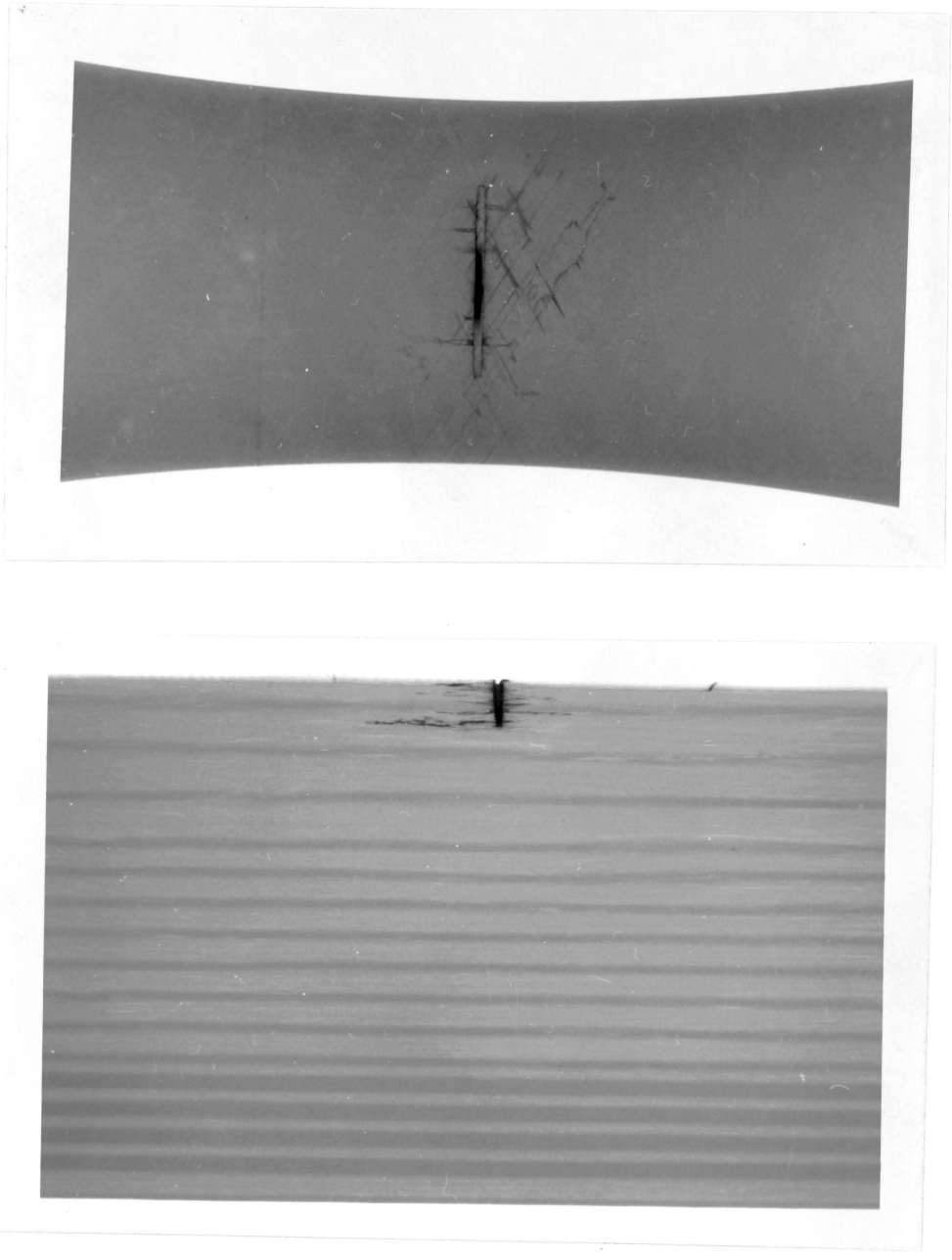

Figure 4. X-Ray Photographs of Typical Specimen at 85% of Failure Load

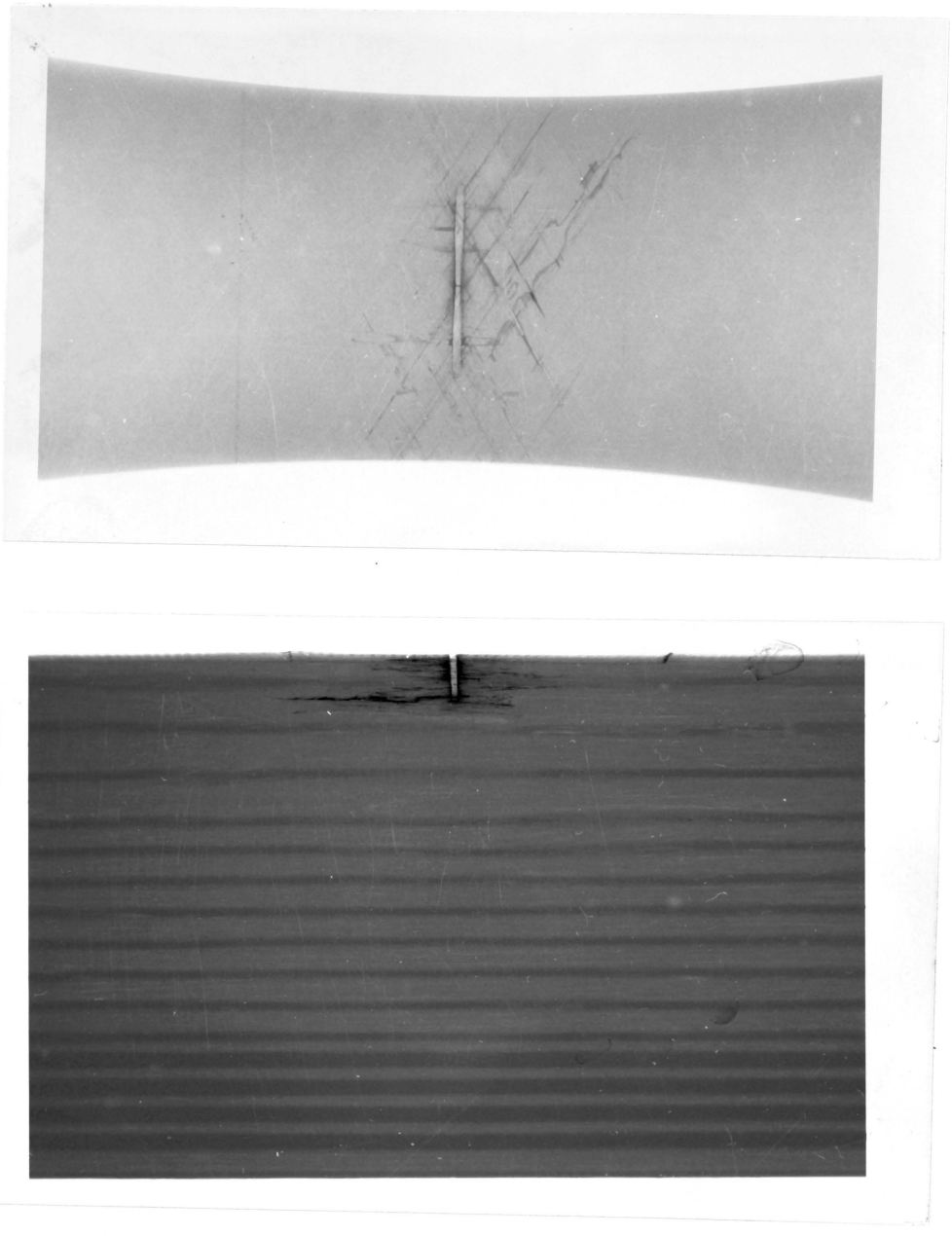

Figure 5. X-Ray Photographs of Typical Specimen at 90% of Failure Load

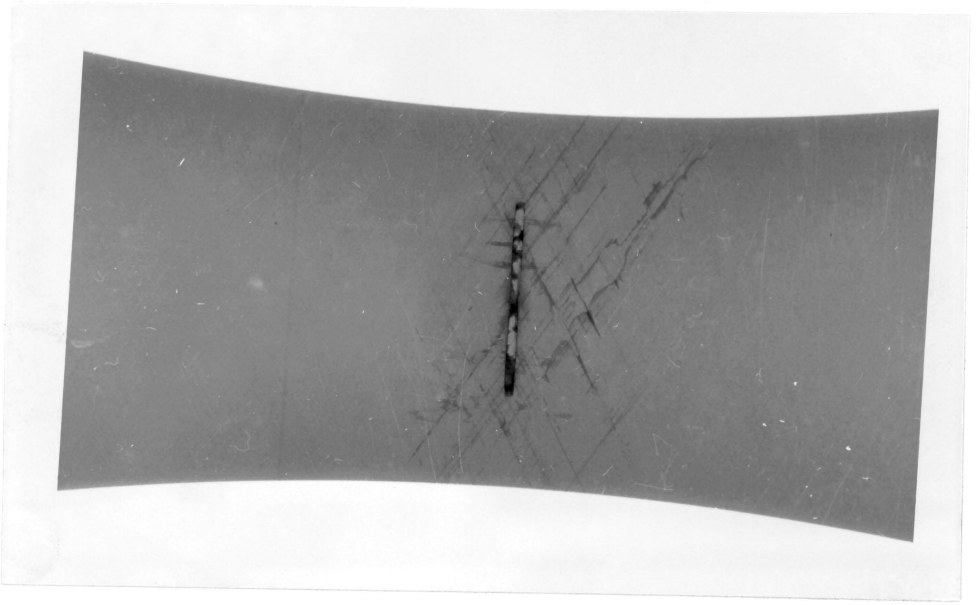

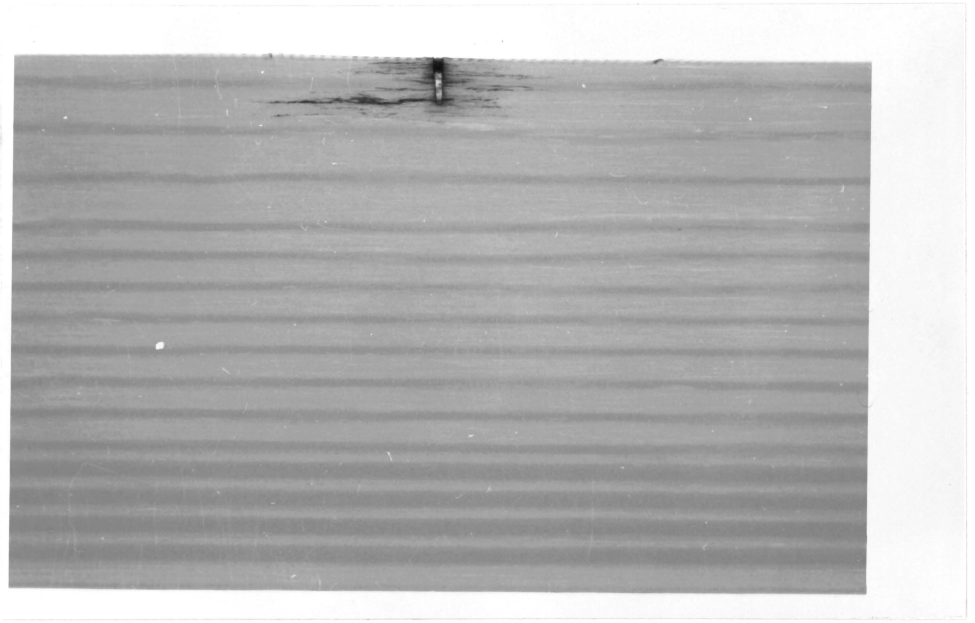

Figure 6. X-Ray Photographs of Typical Specimen at 95% of Failure Load

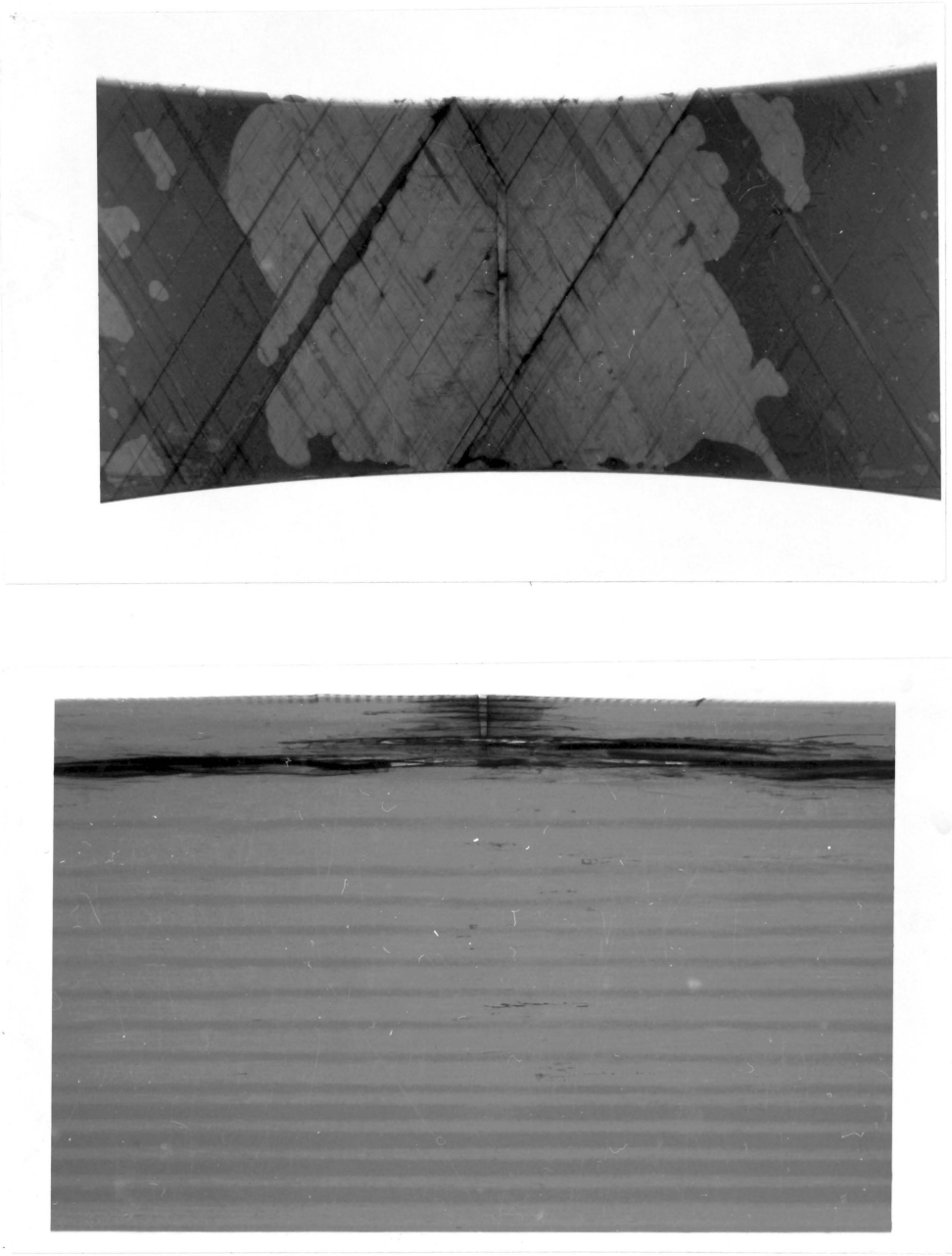

Figure 7. X-Ray Photographs of Typical Specimen at Failure Load

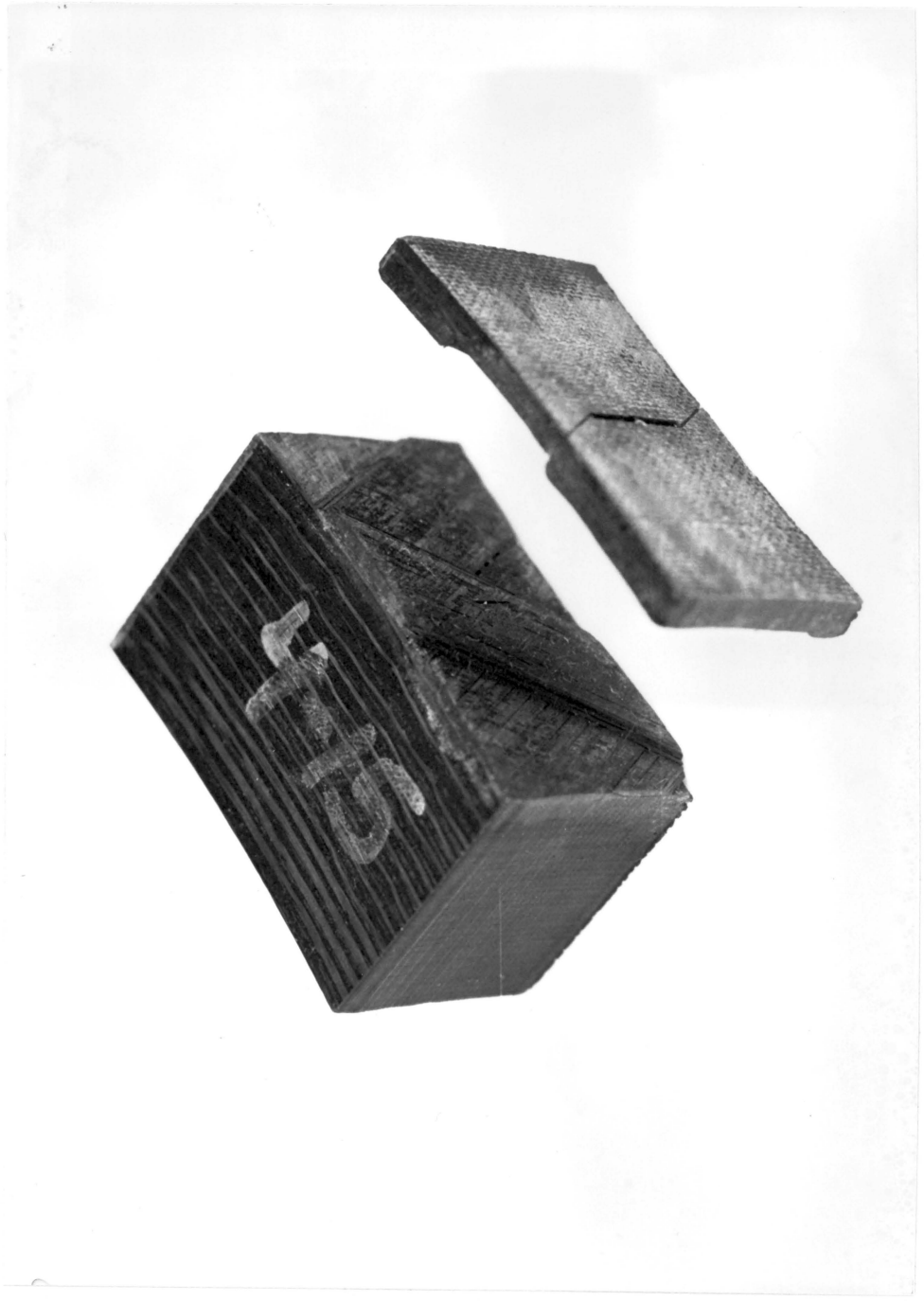

Figure 8. Photograph of Notched Layer Failure Surface

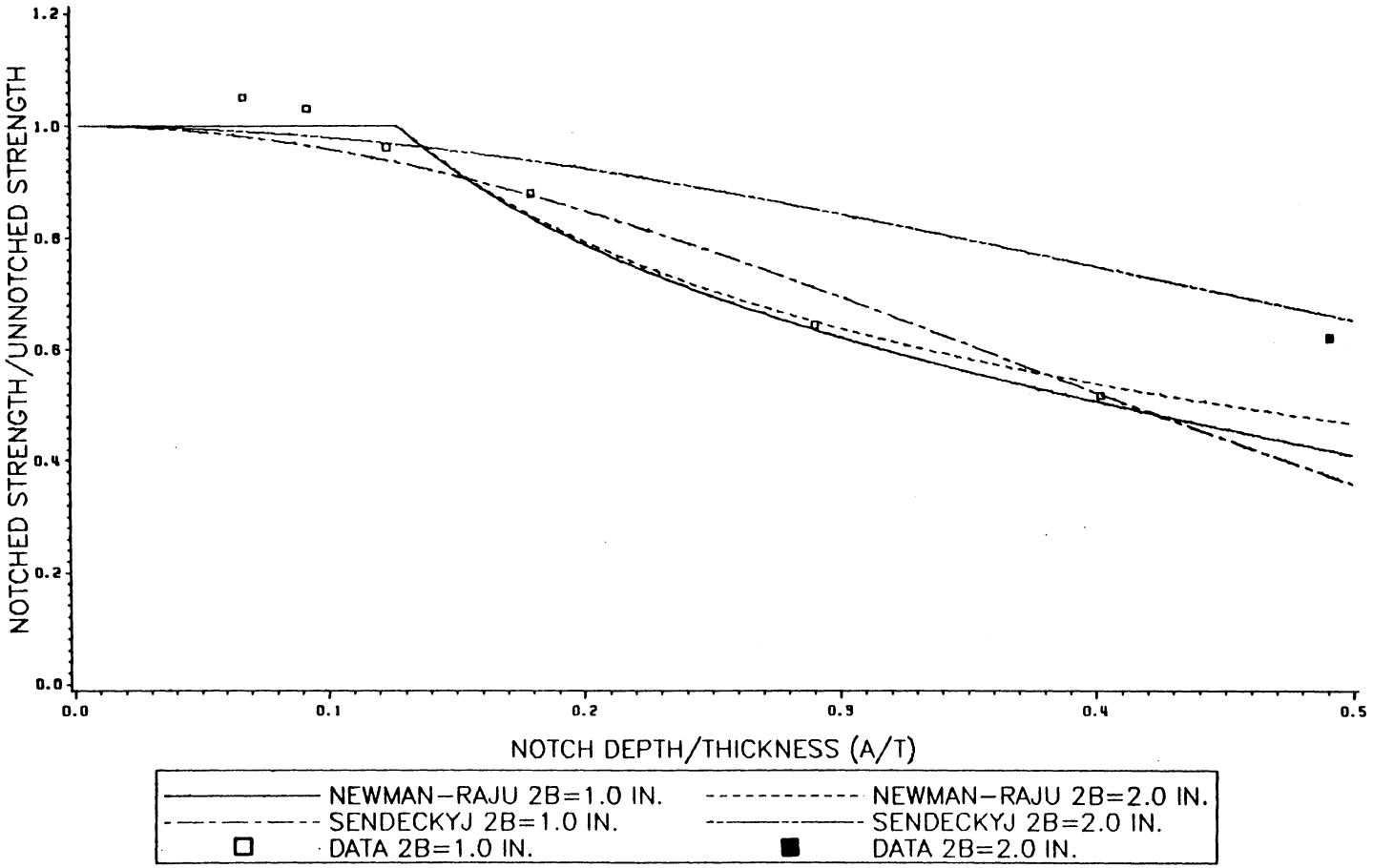

Figure 9. Comparison of Experimental Data to Isotropic Linear-Elastic Prediction for a/c = 2.0

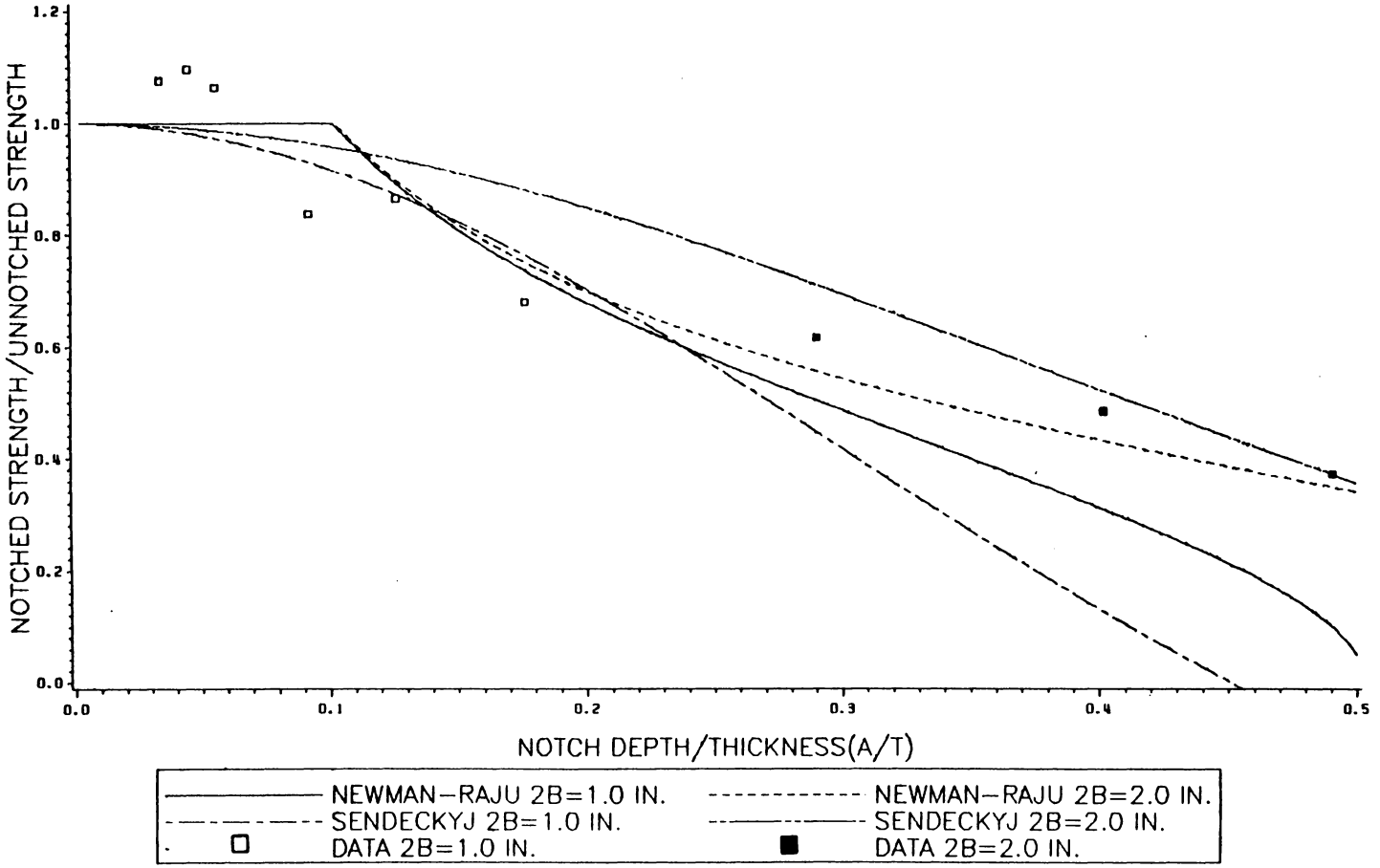

Figure 10. Comparison of Experimental Data to Isotropic Linear-Elastic Prediction for a/c = 1.0

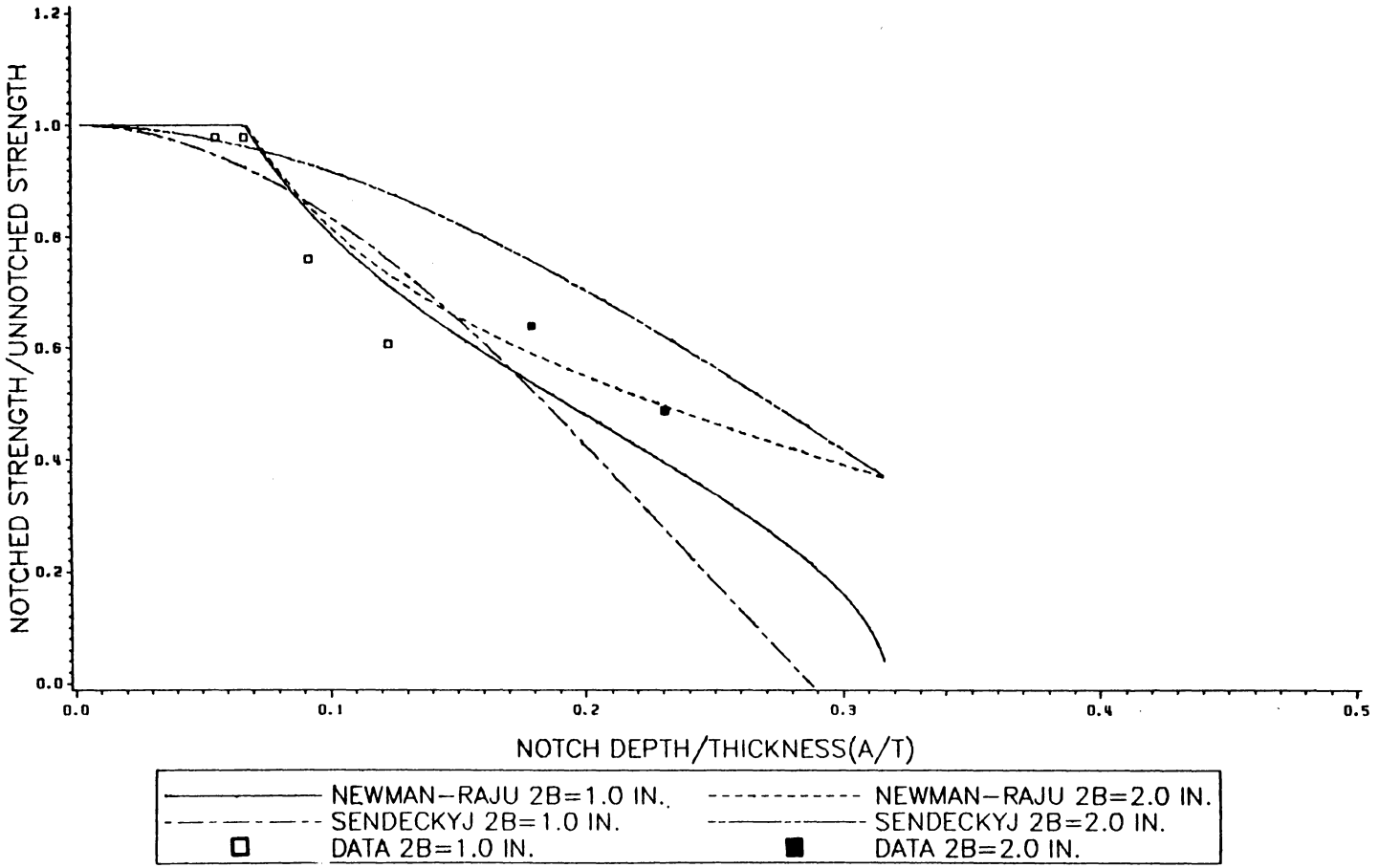

Figure 11. Comparison of Experimental Data to Isotropic Linear-Elastic Prediction for a/c = 0.5

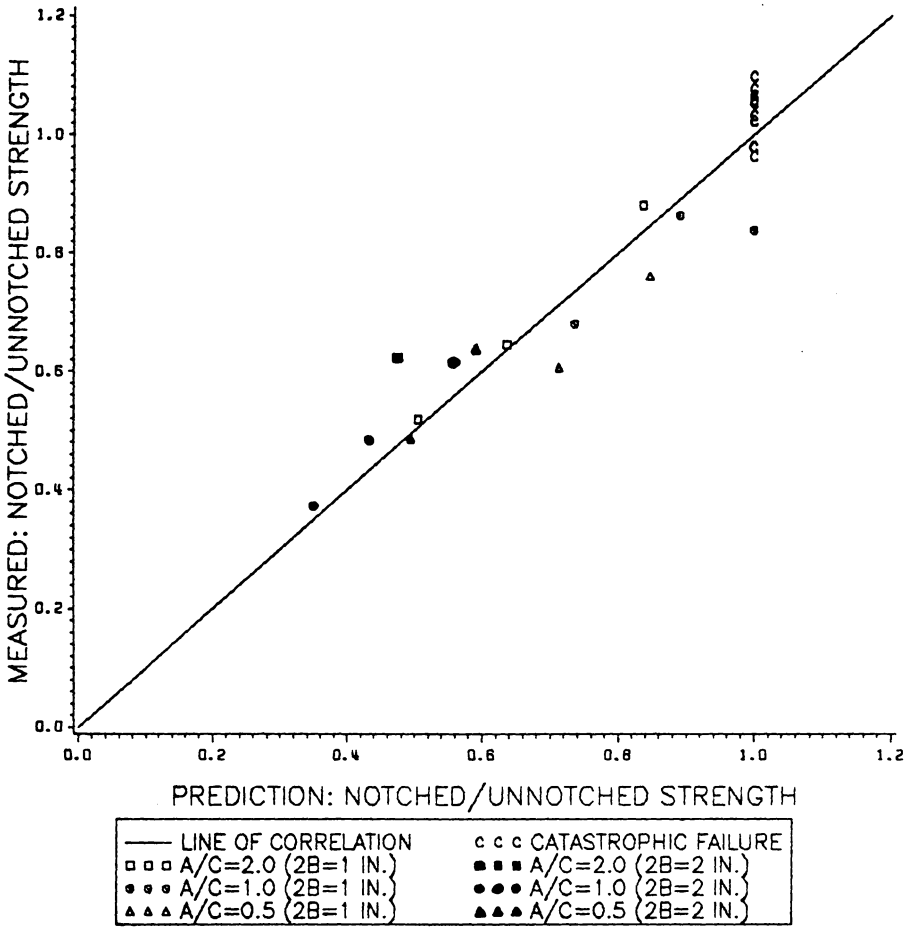

Figure 12. Diagram Illustrating Correlation of Newman-Raju Prediction to Experimental Data

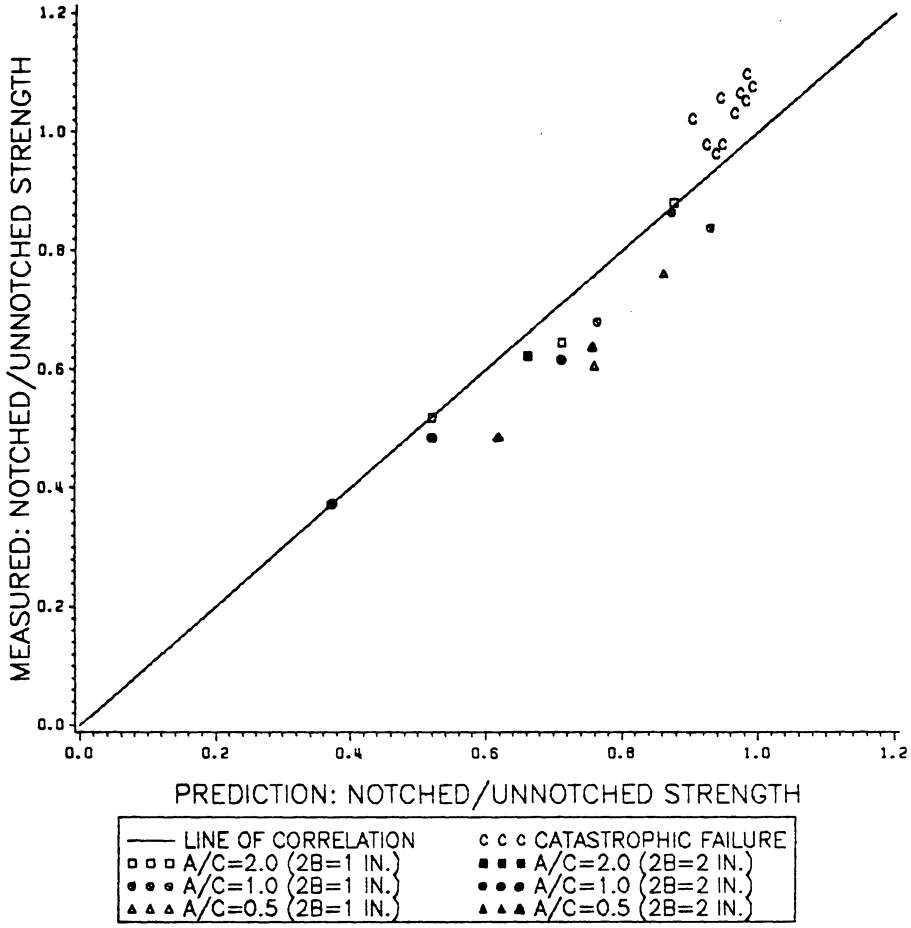

Figure 13. Diagram Illustrating Correlation of Sendeckyj Prediction to Experimental Data

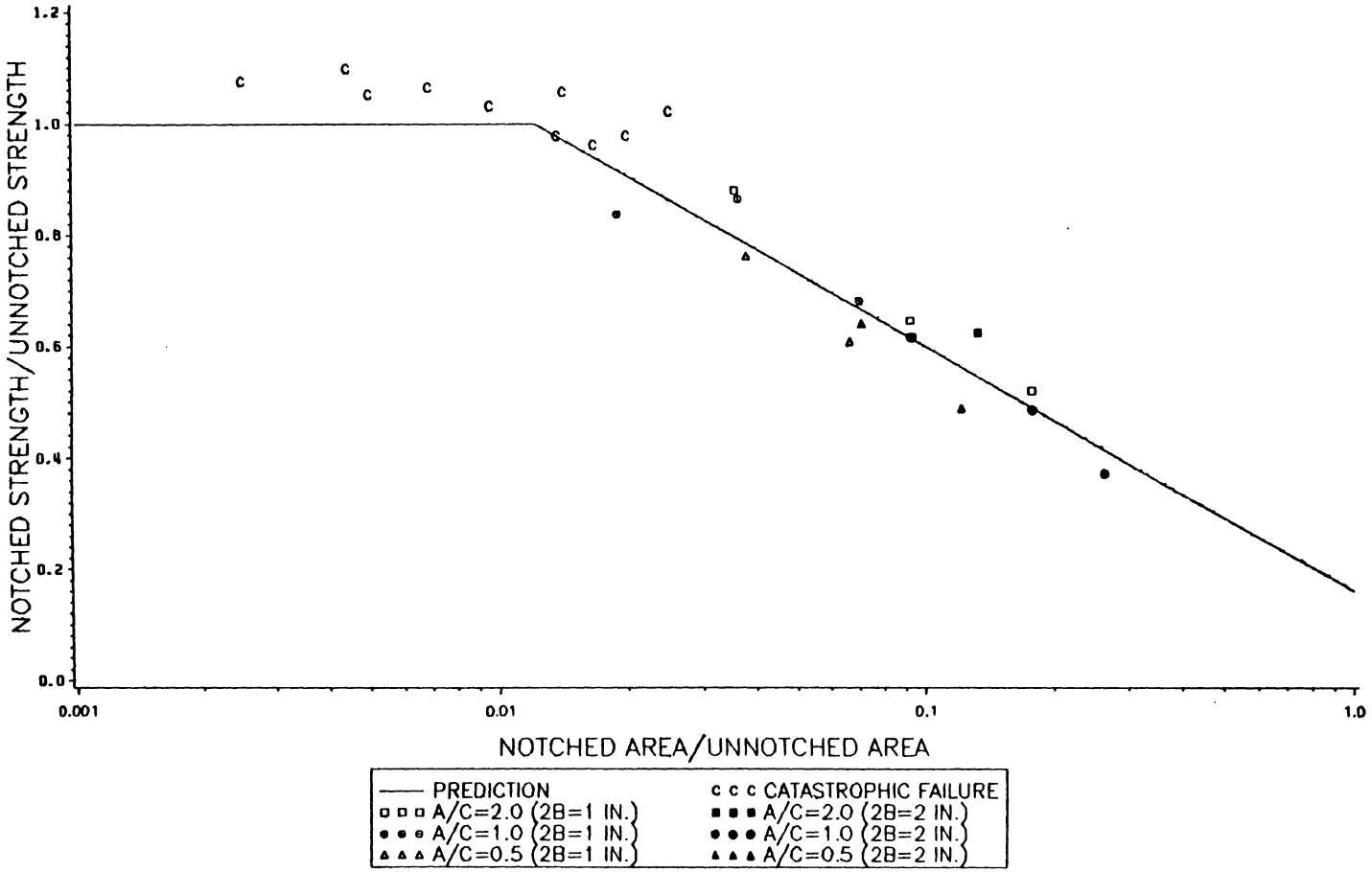

Figure 14. Correlation of Experimental Data and Empirical Notch Area Dependent Solution

The vita has been removed from the scanned document